ELSEVIER

Journal of Contaminant Hydrology 23 (1996) 157–184

JOURNAL OF
Contaminant
Hydrology

A consistent approach for applying numerical boundary conditions for multiphase subsurface flow

Y.S. Wu [a,1], P.A. Forsyth [b,*], H. Jiang [c]

[a] *HydroGeoLogic, Herndon, VA 22070, USA*
[b] *Department of Computer Science, University of Waterloo, Waterloo, Ont. N2L 3G1, Canada*
[c] *Department of Computer Science, University of Waterloo, Waterloo, Ont. N2L 3G1, Canada*

Received 6 February 1995; accepted 4 October 1995

Abstract

The partial differential equations which model multiphase subsurface flow are, in general, of mixed parabolic–hyperbolic type. A consistent and unified approach for handling a wide variety of boundary conditions under all flow conditions is presented. This method is conceptually simple, and numerically efficient. Test computations are presented which demonstrate this method for saturated–unsaturated models, and well as true three-phase simulations. Among the boundary conditions discussed are: seepage face conditions for three-phase problems and multi-node constant-rate pumping wells.

1. Introduction

Simulation of subsurface contamination and remediation involving non-aqueous-phase contaminants (NAPL) requires solution of multiphase flow models (Abriola and Pinder, 1985; Forsyth, 1988; Faust et al., 1989; Kaluarachchi and Parker, 1989; Forsyth, 1991; Falta et al., 1992; Sleep and Sykes, 1993; Panday et al., 1995). Since the partial differential equations which describe multiphase subsurface flow are of mixed hyperbolic–parabolic type, it is not possible, in general, to specify the numerical boundary conditions without reference to the current state of the system. For example, it is possible to specify the composition of injected fluids. However, it is not possible to specify the composition of fluids which are leaving the computational domain.

* Corresponding author.
[1] Present address: Now at Earth Sciences Division, Lawrence Berkeley Laboratory, Berkeley, CA 94720, USA.

SSDI 0169-7722(95)00099-2

In the case of single-phase, saturated, subsurface flow, a constant-pressure (or head) boundary condition is straightforward to specify for a numerical model. However, this is not the case for multiphase flow. This is easy to see if we consider the physical mechanism involved in specifying a constant pressure. Physically, in order to force a constant pressure at a given point, fluid must be injected or removed to keep the pressure constant. In the multiphase case, it is necessary to specify *which* phase pressure is being held constant. In general, more than one phase pressure *cannot* be specified. If two or more phase pressures are specified, then (due to capillary pressure relations) this amounts to specifying a pressure and a phase saturation. This is normally not mathematically correct. If a single-phase pressure is held constant, then it is necessary to specify what fluids are to be injected or removed in order to satisfy this condition. For example, consider a seepage face. Either water or air can be removed, but only air can be injected, in order to maintain the gas-phase pressure at atmospheric.

Constant-rate wells which are screened over several discrete nodes pose yet another problem. In this case, typically only the total liquid rate into the well (if on production) is specified. The allocation of rates to each node must be determined by the model. In the case of horizontal wells, backflow is possible and may have to be taken into account.

Since the flow rate near injection/production wells is large, it is especially important to treat these terms in a fully implicit, fully coupled manner. If these terms are explicit, or lagged an iteration, this will result in poor numerical performance.

In saturated–unsaturated models, it is necessary to determine the liquid level in the wellbore for any well pumping at a constant rate. We will demonstrate how this can be modelled in a conceptually simple manner.

The objective of this paper is to present a consistent, unified approach to handling all these types of boundary conditions. For ease of exposition, we concentrate on multiphase flow with no mass transfer between phases. We also assume that each phase consists of a single chemical component. The approach used here can be easily extended to the full compositional formulation. The numerical method allows for straightforward implementation and new types of boundary conditions are easily handled. Several different methods for modelling constant-rate wells are discussed. Numerical examples are presented for various boundary conditions. In particular, we are able to use a very straightforward method to model the complex behavior of multiphase flow near a seepage face.

2. Formulation

We consider multiphase flow with no mass transfer between the phases, and each phase is assumed to be composed of a single component. In the special case of two-phase air–water flow with constant air pressure, this reduces to the usual passive air-phase (saturated–unsaturated) flow model.

The three phases considered here are water (w), air (a) and nonaqueous (n). Conservation of phase l then implies:

$$\frac{\partial}{\partial t}(\phi S_l \rho_l) = -\nabla \cdot (\rho_l V_l) + \rho_l q_l' \tag{1}$$

where the velocity of each phase l is given by

$$\boldsymbol{V}_l = -\boldsymbol{K} \cdot \lambda_l (\nabla P_l - \rho_l g \nabla D) \tag{2}$$

and where S_l = saturation of phase l; P_l = pressure of phase l; ρ_l = mass density of phase l; $\boldsymbol{K}$ = absolute permeability tensor; $\lambda_l = k_{rl}/\mu_l$ is the mobility; μ_l = viscosity of phase l; k_{rl} = relative permeability of phase l; D = depth; g = gravitational acceleration; q_l' = source/sink term for phase l due to wells.

We also have the usual capillary pressure and phase saturation constraints (Forsyth, 1991; Wu et al., 1994).

3. Discretization

A Galerkin finite-element method is used to discretize the equations (Eq. 1). An influence coefficient technique is employed to handle the non-linearities in the flow terms (Huyakorn et al., 1984). The time discretization is carried out with a backward Euler method, and mass lumping is used for the mass accumulation term. Further details about this method can be found in Forsyth (1991, 1993), Forsyth and Shao (1991), and Letniowski and Forsyth (1991).

Let N_i be the usual Lagrange polynomial C^0 basis functions, where:

$$N_i = \begin{cases} 1 & \text{at node } i \\ 0 & \text{at all other nodes} \end{cases} \tag{3a}$$

$$\sum_j N_j = 1 \quad \text{everywhere in the solution domain} \tag{3b}$$

For convenience, we define $\psi_l = P_l - \rho_l g D$. Then, P_l, ψ_l and S_l are approximated by, respectively:

$$P_l = \sum_j P_{lj} N_j \tag{4a}$$

$$\psi_l = \sum_j \psi_{lj} N_j = \sum_j \left(P_{lj} - P_{lj} g D_j \right) N_j \tag{4b}$$

$$S_l = \sum_j S_{lj} N_j \tag{4c}$$

If N denotes the time level, then the final discrete equations for phase l = w, a, n are:

$$\left\{ [\phi S_l \rho_l]_i^{N+1} - [\phi S_l \rho_l]_i^N \right\} \frac{V_i}{\Delta t} = \sum_{j \in \eta_i} (\rho_l \lambda_l)_{(i\,j+1/2)}^{N+1} \gamma_{ij} \left(\psi_{lj}^{N+1} - \psi_{li}^{N+1} \right)$$

$$+ (\rho_l q_l')_i^{N+1} V_i + \int_s N_i (\rho_l \boldsymbol{V}_l)^{N+1} \cdot \hat{n} \, \mathrm{d}s \tag{5}$$

where

$$V_i = \int_v N_i \mathrm{d}v \tag{6a}$$

$$\psi_{li}^{N+1} = P_{li}^{N+1} - \rho_{l,i\,j+1/2}^{N+1} g D_i \tag{6b}$$

$$\rho_{l,i\,j+1/2} = (\rho_{l,i} + \rho_{l,j})/2 \tag{6c}$$

and the γ_{ij} are given by

$$\gamma_{ij} = -\int_v \nabla N_i \cdot \boldsymbol{K} \cdot \nabla N_j \mathrm{d}v \tag{7}$$

Here η_i is the set of neighbour nodes of node i such that γ_{ij} are nonzero.

In Eq. 5, the term:

$$\int_s N_i (\rho_l \boldsymbol{V}_l)^{N+1} \cdot \hat{n} \mathrm{d}s \tag{8}$$

represents the flux into the domain due to specified flux (or pressure) boundary conditions. (Recall that a specified pressure can always be enforced by injecting or producing mass into a node.)

Since this term simply represents mass inflow or outflow, we can lump this boundary flux in with the flux due to wells to get a composite source/sink term:

$$q_{li}^{N+1} = (\rho_{li} q'_{li})^{N+1} V_i + \int_s N_i (\rho_l \boldsymbol{V}_l)^{N+1} \cdot \hat{n} \mathrm{d}s \tag{9}$$

Therefore the final discrete equations are:

$$\left\{ [\phi S_l \rho_l]_i^{N+1} - [\phi S_l \rho_l]_i^N \right\} \frac{V_i}{\Delta t} = \sum_{j \in \eta_i} (\rho_l \lambda_l)_{(i\,j+1/2)}^{N+1} \gamma_{ij} \left(\psi_{lj}^{N+1} - \psi_{li}^{N+1} \right) + q_{li}^{N+1} \tag{10}$$

There are various possibilities for the term $(\rho_l \lambda_l)_{(i\,j+1/2)}$ in Eq. 10. We will use upstream weighting (ups) in this work.

$$(\rho_l \lambda_l)_{\mathrm{ups}(i,j)} = \begin{cases} (\rho_l \lambda_l)_i^{N+1} & \text{if} \quad \gamma_{ij} \left(\psi_{lj}^{N+1} - \psi_{li}^{N+1} \right) < 0 \\ (\rho_l \lambda_l)_j^{N+1} & \text{if} \quad \gamma_{ij} \left(\psi_{lj}^{N+1} - \psi_{li}^{N+1} \right) > 0 \end{cases} \tag{11}$$

For true two-phase (non-constant air-phase pressure) problems, upstream weighting can be shown to converge to the physically correct solution (Sammon, 1988). As demonstrated in Aziz and Settari (1979), central weighting may cause convergence to incorrect solutions in multiphase flow situations. Further discussion of the effects of upstream, fully implicit weighting methods for multi-phase flow is given in Unger et al. (1996).

Note that the discrete equations (10) have the same form regardless of the dimensionality of the system or the type of basis function used. In fact, Eqs. 5 are also valid if a finite volume discretization is used (Falta et al., 1989, 1992). In this case, the V_i's are the actual geometric volumes associated with the node, and γ_{ij} is the inter-facial area

divided by the distance between nodes i and j. The surface integral (8) can simply be regarded as the total mass flow into a finite volume on the edge of the computational domain. In the finite-element case, the surface integral can be interpreted as the total mass flow into a node on the edge of the domain. The area associated with node i is simply:

$$A_i = \int_s N_i \mathrm{d}s \tag{12}$$

Since the discrete equations have the same form for finite-element or finite-volume discretizations, the method we will describe for handling the boundary conditions can be used with either type of discretization.

4. Single-node wells

We first describe the method for modelling wells which are screened over a single computational node.

Suppose we have a constant-pressure production well at node i. In the following we will drop the superscript $(N+1)$ for notational convenience; it will be assumed that all boundary condition terms are evaluated fully implicitly. It is reasonable to assume that the capillary pressure is zero in the wellbore, so that the sink terms have the form (where P_s is the specified pressure):

$$q_{li} = \mathrm{WP}_i \lambda_{li} \rho_{li} \min\left[0,(P_s - P_{li})\right] \tag{13}$$

The term WP_i is the productivity index. If the mesh spacing in the direction perpendicular to the wellbore is large compared to the actual wellbore radius, then WP_i can be determined by assuming that the flow is radial near the wellbore. The methods used in Peaceman (1983, 1990), Collins et al. (1992), Fung et al. (1992), and Forsyth (1994) can then be used to determine the expression for WP_i. Assume that the discretization grid is composed of brick elements, with the wellbore being along one of the brick axes. If the permeability tensor is diagonal,

$$\boldsymbol{K} = \begin{pmatrix} k_x & 0 & 0 \\ 0 & k_y & 0 \\ 0 & 0 & k_z \end{pmatrix} \tag{14}$$

and, we suppose that the wellbore is along the x-axis of the brick element, then:

$$\mathrm{WP}_i = \frac{2\pi k' h_i \sum_{j \in \eta_i'} \gamma_{ij}}{\sum_{j \in \eta_i'} \gamma_{ij} \log\left(r_j'/r_w'\right) - 2\pi k' h_i} \tag{15}$$

where

$$r_w' = \tfrac{1}{2} r_w \left[\left(\frac{k_y}{k_z} \right)^{1/4} + \left(\frac{k_z}{k_y} \right)^{1/4} \right]$$

$$r_j' = \left(\frac{z_j^2 k'}{k_z} + \frac{y_j^2 k'}{k_y} \right)^{1/2}$$

$$k' = \left(k_z k_y \right)^{1/2}$$

$$h_i = \frac{\| x_i - x_\alpha \|}{2} + \frac{\| x_i - x_\beta \|}{2}$$

where r_w is the actual wellbore radius; x_j and y_j are the x- and y-coordinates, respectively, of node j; η_i' are those neighbour nodes of node i which are not along the wellbore direction; and α and β are neighbours of node i along the wellbore. The above expression is a three-dimensional generalization of the expressions given in Fung et al. (1992). For further details, the reader is referred to Peaceman (1983, 1990), and Fung et al. (1992). If the well is screened over a length less than h_i is Eq. 15, then WP_i should be reduced by the factor:

$$\frac{(\text{actual screened length})}{h_i} \tag{16}$$

Note that we have forced mass outflow for all phases in Eq. 13, i.e. we do not allow any inflow for a single-node production well. Also, in Eq. 13, the pressure drop term for each phase uses the phase pressure. If the node spacing is large compared to the wellbore radius, then it is common in petroleum engineering to assume the same pressure drop for all phases. It has been shown in (Aziz and Settari, 1979) that for petroleum engineering applications, this results in a negligible error in most cases. However, this may not be the case in near-surface flow situations.

Suppose that we wish to model a well which produces at a constant liquid rate Q_{liq}. Of course, it is not always physically possible to produce liquids. For example, water and NAPL may be at residual saturations. Therefore, it is usual to specify a constant liquid rate subject to a minimum well pressure P_{smin}.

In this case, the mass production of each phase is given by Eq. 13, with P_{s} given by:

$$P_{\mathrm{s}}' = \frac{Q_{\mathrm{liq}} + \mathrm{WP}_i \left(\lambda_{\mathrm{w}i} \rho_{\mathrm{w}i} P_{\mathrm{w}i} + \lambda_{\mathrm{n}i} \rho_{\mathrm{n}i} P_{\mathrm{n}i} \right)}{\mathrm{WP}_i \left(\lambda_{\mathrm{w}i} \rho_{\mathrm{w}i} + \lambda_{\mathrm{n}i} \rho_{\mathrm{n}i} \right)} \tag{17a}$$

$$P_{\mathrm{s}} = \max\left(P_{\mathrm{smin}}, P_{\mathrm{s}}' \right) \tag{17b}$$

It is usual to inject a single phase only. For example, a constant-pressure water injector would have the form:

$$q_{\mathrm{w}i} = \mathrm{WP}_i \lambda_{\mathrm{w}} \left(S_{\mathrm{w}} = 1 \right) \rho_{\mathrm{w}} \left(P_{\mathrm{s}} \right) \max\left[0, \left(P_{\mathrm{s}} - P_{\mathrm{w}i} \right) \right] \tag{18}$$

Note that the mobility λ_{w} and the density are evaluated at the assumed upstream

conditions in the wellbore. If a constant-rate water injector Q_w with a maximum well pressure P_{smax} is specified then Eq. 18 is used with P_s given by:

$$P_s' = \frac{Q_w}{WP_i[\lambda_w(S_w = 1)\rho_w(P_s)]} + P_{wi} \tag{19a}$$

$$P_s = \min(P_{smax}, P_s') \tag{19b}$$

5. Multinode wells

There are three methods for handling multinode wells. Undoubtedly the most accurate method involves discretizing the wellbore.

5.1. Discrete wellbore

Suppose we have a set of nodes $i \in w$ which are the nodes in the original computational domain along the length of the wellbore. For each node $i \in w$ we add a new node $j \in w'$ which is physically within the wellbore. This new node j can be imagined to be at the same physical location as the node i on the original grid. Each new node has its own pressure and saturation values distinct from the adjacent grid node. The volume of nodes $j \in w'$ is the actual volume of the discrete length of the wellbore. Since nodes $j \in w'$ are in the wellbore, we assume laminar one-dimensional fluid flow between nodes in w'. Since laminar, multiphase flow has the same form as Darcy flow, the discrete equations connecting nodes in w' have the same form as Eqs. 5. It is only necessary to make some modifications to the expressions for the density and absolute permeabilities (Collins et al., 1992). The capillary pressure is assumed to be zero and the relative permeabilities are linear functions for nodes in w'.

It then remains to determine the flow into node j (a wellbore node) from node i (its nearest grid node). If we assume that the flow is radial near the wellbore, then we can use the Eq. 15 for the productivity index, so that flow of phase l from node i to node j (flow_{lij}) is given by:

$$\text{flow}_{lij} = WP_i(\lambda_l \rho_l)_{ij+1/2}(P_{li} - P_{lj}) \tag{20}$$

Then, we assume that the pump is located at a node $k \in w'$. At node k, we use the usual single-node sink and source expressions such as Eqs. 13 and 18, respectively. Fluid then flows from the grid nodes into the wellbore, and then into the sink node, and out of the computational domain.

Note that no assumptions are made concerning the direction of flow at each grid node $i \in w$. This means that backflow can occur at various points along the wellbore. However, the total flow as specified at the pump node in the wellbore has the correct sign. Backflow can actually occur for horizontal wells, and for vertical wells if the absolute permeability contrast between layers is very high.

Since all these additional equations have the same form as the original discrete equations (5), it is actually very straightforward to modify an existing code to handle multinode wells in this manner.

Of course, since the wellbore node has a very small volume, if the flow rates are large, this may cause some difficulty for the Newton iteration in multiphase flow problems. This can be alleviated by increasing the volume of the wellbore nodes by 10^2–10^3. This has the effect of adding a pseudo wellbore storage effect, which dampens out oscillations in the Newton iteration. Unless one is interested in very small-scale transient behaviour, this pseudo wellbore storage has almost no effect on the computed solution (Forsyth, 1994).

In the case of saturated–unsaturated flow (passive air-phase approximation), we cannot, of course, set the capillary pressure to zero in the wellbore. However, if we use an air–water capillary pressure function P_{caw} of the form:

$$P_{\mathrm{caw}} = \alpha(1 - S_{\mathrm{w}}) \tag{21}$$

where $\alpha \approx 10^{-3}$ kPa, then for practical purposes, the capillary pressure is almost zero, but the non-zero slope in Eq. 21 allows the usual passive air-phase equations to be used. If the wellbore intercepts the water table, then the wellbore nodes will be fully saturated below the water level in the wellbore. At a node height corresponding to the water level, the wellbore node saturation will be at some value between zero and one, and all nodes above this point will have zero water saturation. This simulates the correct behaviour of a near-surface well.

5.2. Single-node wellbore

For problems where it can be assumed that the fluid composition in the wellbore is sensibly constant along the length of the wellbore (i.e. horizontal wells, vertical wells below the water table, injection wells, vapour extractors in the vadose zone), it is unnecessary to discretize the wellbore. Instead, a single virtual node is used to represent the wellbore. As for the Discrete Wellbore model, we assume a set of nodes $i \in w$ which are nodes in the original grid along the length of the wellbore. The wellbore is represented by a single new node j, having the volume of the screened length of the well. The pump is located at a given depth D_{p} in the well. For any node $i \in w$, flow from node i to the single well node j is given by:

$$\mathrm{flow}_{lij} = \mathrm{WP}_i(\lambda_l \rho_l)_{i\,j+1/2}\left(P_{li} - P_{lj} - \rho_{\mathrm{f}} g\left(D_i - D_{\mathrm{p}}\right)\right) \tag{22}$$

where ρ_{f} is the density of the fluid mixture in the wellbore. Note that the gravity term must be included in Eq. 22 since the grid nodes i and pump location may be at different depths. A source/sink expression of the form [(18),(13)] is added to the mass-balance expression for the virtual node j to force the correct total rate of fluid injection/production from the well. Since there is no flow being simulated within the wellbore, the numerical problem is not as stiff as for the Discrete Wellbore model. This model does permit backflow.

5.3. No Backflow model

If it can safely be assumed that no backflowing layers will occur, then the Single-Node model can be simplified further. Instead of introducing an additional node, having node

pressures, saturations and a finite volume, for each multinode well, we add an additional unknown P_s. Flow from a grid node $i \in w$ into the well (a production well is assumed here) is given by:

$$\text{flow}_{li\text{s}} = \text{WP}_i(\lambda_l \rho_l)_i \min\left[0,\left\{P_{li} - P_s - \rho_f g(D_i - D_p)\right\}\right] \tag{23}$$

The well pressure P_s is determined by an additional constraint equation. For example, if the total water rate Q_{tw} is specified, then the additional constraint equation is:

$$Q_{tw} = \sum_{i \in w} \text{flow}_{w i s} \tag{24}$$

Max/min pressure constraints can be added to this equation in a similar manner as in Eqs. 17 and 19. This technique is probably the most common method used in the petroleum industry. However, the solution may not always be physically correct, since any potentially backflowing layers have their flow set to zero. Nevertheless, the correct total fluid injection/production rates are always satisfied exactly (if the max/min pressure constraints are not violated).

5.4. Mobility Allocation model

Historically, this method was used in the petroleum industry before general sparse solvers for the Jacobian matrix were available. This method assumes that the pressure drop between a node adjacent to the wellbore and the wellbore is a constant along the wellbore. For example, suppose nodes $i \in w$ are the grid nodes along the screened length of the wellbore, and that the total volumetric liquid production rate Q_{liq} is specified. Then (l = w, n):

$$q_{li} = \rho_{li} \frac{\text{WP}_i \lambda_{li} Q_{\text{liq}}}{\sum_{j \in w} \text{WP}_j(\lambda_{\text{w}j} + \lambda_{\text{n}j})} \tag{25}$$

This scheme is easy to implement, but may result in physically incorrect solutions, especially for heterogeneous systems.

6. Nonwell boundary conditions

In order to model constant-pressure nodes, seepage faces, and so on, we continue with the philosophy of simulating all boundary conditions using mass source/sink terms. For example, suppose we wish to model a constant water pressure (P_{wb}) boundary at node i, due to a large aquifer. In this case we add the following source/sink term to node i

$$q_{li} = \text{WP}'_i \lambda_{li} \rho_{li} \min\left[0,(P_{\text{wb}} - P_{li})\right] \quad (l = \text{g, n}) \tag{26a}$$

$$q_{\text{w}i} = \text{WP}'_i \lambda_{\text{w}i} \rho_{\text{w}i} \min\left[0,(P_{\text{wb}} - P_{\text{w}i})\right] + \text{WP}'_i \lambda_{\text{w}}(S_{\text{w}} = 1) \rho_{\text{w}}(P_{\text{wb}}) \max\left[0,(P_{\text{wb}} - P_{\text{w}i})\right] \tag{26b}$$

Note that we allow any phase to flow out of node i, but only water to flow into node i. We have made the assumption that any phase which flows into the aquifer is immediately dispersed. This is essentially the best model (for a node adjacent to an aquifer) that can be developed without adding nodes in the aquifer.The factor WP_i' in Eq. 26 does not have any physical significance. It must be selected large enough so that the converged solution for P_{wi} is very close to the specified pressure P_{wb}. It cannot of course be exactly equal to P_{wb}, but can be made as close as desired by increasing WP_i'. However, if WP_i' is too large, this can cause problems for the Newton iteration. Based on our numerical experience, we have found that if

$$WP_i' = WP_i * \text{LARGE} \quad (\text{LARGE} \approx 10^2 - 10^3) \tag{27}$$

where WP_i is given by Eq. 15, then the node pressure $P_{wi} = P_{wb}$ to 3–4 figures. If LARGE $> 10^3$, then there is no observable difference in the solution (i.e. rates, nodal pressures, saturations), but usually the number of Newton iterations increases.

Although at first sight is not obvious why the solution should be insensitive to the precise value of LARGE after a certain point, this can be explained as follows, although

$$P_{wi} \to P_{wb} \quad \text{as} \quad \text{LARGE} \to \infty \tag{28}$$

the product of:

$$WP_i' \lambda_{wi} \rho_{wi} (P_{wb} - P_{wi}) \tag{29}$$

approaches a finite limit.

An interesting special case occurs near a seepage boundary. We model a seepage face by assuming that air can flow in and out of the computational domain, so that the air pressure $P_a = P_{ab} = 100$ kPa. Water and nonaqueous phases can only flow out. So, at any node i along a seepage face, the source/sink terms are:

$$q_{li} = WP_i' \lambda_{li} \rho_{li} \min[0, (P_{ab} - P_{li})] \quad (l = w, n) \tag{30a}$$

$$q_{ai} = WP_i' \lambda_{ai} \rho_{ai} \min[0, (P_{ab} - P_{ai})] + WP_i' \lambda_a (S_a = 1) \rho_a (P_{ab}) \max[(0, (P_{ab} - P_{ai})] \tag{30b}$$

Eqs. 30 can be explained as follows: we can imagine that there is a pseudo node (p) adjacent to the seepage face node located outside the domain. This node is not in a porous medium, so that $P_{ap} = P_{np} = P_{wp} = P_{ab}$. The air phase is free to move from node i to node p, and vice versa. However, we can imagine that any water or nonaqueous phase which enters the pseudo node is immediately removed (i.e. the liquid phases seep down the seepage face under the influence of gravity). Consequently, no water or nonaqueous phase can flow from node p to node i. We then take the limit as the distance between node i and node p goes to zero.

At a given liquid saturation with nonzero liquid–gas capillary pressure, and assuming a mobile air phase, then the air-phase pressure at node i will be virtually equal to P_{ab}. Due to capillary pressure effects, no liquid will flow out, until the air saturation is reduced to its residual value (which is typically zero). At this point, if the nonaqueous-phase saturation is such as to give a mobile nonaqueous phase and a nonzero water–nonaqueous phase capillary pressure, then only the nonaqueous phase will flow out,

until the nonaqueous-phase saturation is reduced to near the residual value. This phenomenon is called the outlet effect (Settari, 1973; Aziz and Settari, 1979). Note that as the nonaqueous phase approaches the residual value, it can no longer be assumed that the pressure in the nonaqueous phase is exactly equal to atmospheric pressure (due to the very small relative permeability as residual nonaqueous-phase saturation is approached). In fact, it is possible to have simultaneous outflow of both phases. We will give some computational examples which illustrate this point.

7. Solution of the algebraic equations

Typically, the discrete nonlinear algebraic equations are solved using a full Newton, fully coupled approach. If a numerical method for constructing the Jacobian is used (Forsyth et al., 1995), then it is a straightforward matter to ensure that the Jacobian contains all the required derivatives. Even if a structured grid is used, the Jacobian matrix will not, in general, have a banded structure. This is because the presence of a constant-rate well, screened over several nodes, will result in *non-neighbour* connections appearing in the Jacobian. This does not pose any difficulties for the matrix solution if modern sparse techniques are used. We typically use an incomplete LU factorization (ILU) (D'Azevedo et al., 1992) with CGSTAB acceleration (van der Vorst, 1992).

However, it was sometimes suggested (in the petroleum literature) that the non-neighbour terms in the Jacobian could be dropped from the Jacobian (i.e. lagged one iteration). This would make the Jacobian matrix easier to construct, and allow the use of band solvers. For example, if the No Backflow model is used (see Section 5.3), then this method effectively lags the evaluation of P_s one iteration, i.e. all derivatives with respect to P_s are ignored. This same idea can also be used for modelling other boundary conditions (i.e. seepage faces). We will refer to this approach as Partial Jacobian, since some of the Jacobian entries have been ignored.

In general, we will always use a fully coupled, full Newton method. For some of the numerical examples, we will give some results using the Partial Jacobian method, in order to illustrate the advantages of a full Newton approach.

8. Numerical examples

There are clearly too many different cases of source/sink terms as outlined in Sections 4–6 to give an example of each case. We will give some representative examples to illustrate the flexibility and generality of our approach, and discuss some interesting special cases at length.

8.1. Saturated–unsaturated flow

Saturated–unsaturated flow is, of course, a special case of multi-phase flow, and all the methods described in Sections 4–6 can be used in this case as well.

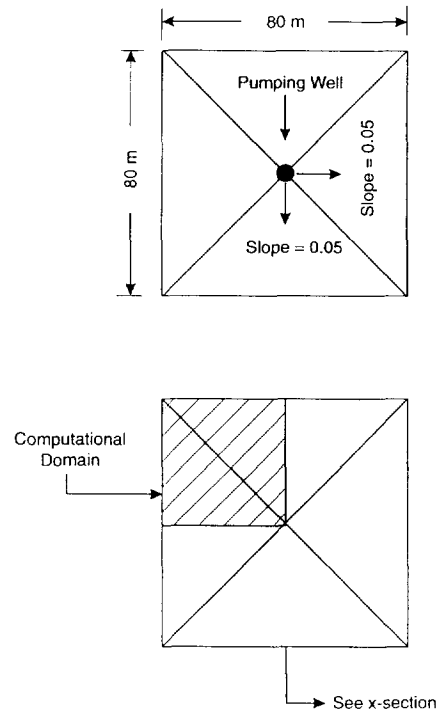

Fig. 1. Top view of the three-dimensional layered waste cover design, clay layer.

Fig. 1 shows the top view of the clay cap for a three-dimensional layered waste cover design. This shape is similar to that used in Meyer (1993) in the context of a capillary barrier waste cover. A cross-section of the pyramid shape (as indicated in Fig. 1) is

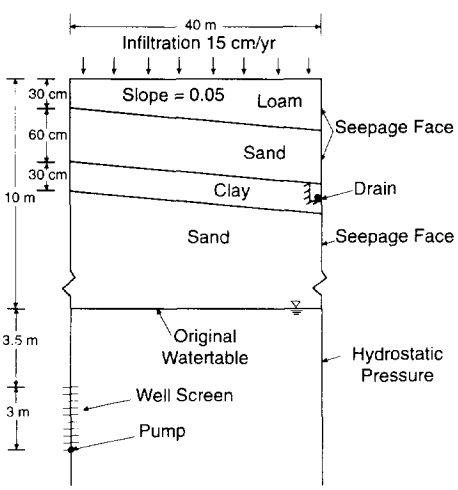

Fig. 2. Cross-section of three-dimensional waste cover.

Table 1
Material properties

Zone	$K_x = K_y = K_z$ (m^2)	ϕ	S_{wr}	α (cm^{-1})	β
Loam	$0.17 \cdot 10^{-11}$	0.452	0.0752	0.043	1.246
Sand	$0.67 \cdot 10^{-11}$	0.345	0.046	0.0634	1.53
Clay	$3.0 \cdot 10^{-15}$	0.475	0.223	0.0304	1.187

shown in Fig. 2. The surface of the design was flat, and the pyramid shape was used for the sand and clay layers. We will assume that the constitutive properties are of the van Genuchten (1980) form:

$$P_{caw} = \frac{\rho_w g}{\alpha}\left[\left(\bar{S}_w\right)^{-1/\gamma} - 1\right]^{1/\beta} \tag{31}$$

where P_{caw} is the air–water capillary pressure; and

$$\bar{S}_w = \frac{S_w - S_{wr}}{1 - S_{wr}}$$

$$\gamma = 1 - \beta^{-1}$$

The relative permeabilities are given by:

$$k_{rw} = \left(\bar{S}_w\right)^{1/2}\left[1 - \left\{1 - \left(\bar{S}_w\right)^{1/\gamma}\right\}^{\gamma}\right]^2 \tag{32}$$

The material properties are given in Table 1.

The idea of this waste cover design is to deflect infiltration away from the waste buried in the sand. Water will be deflected by the clay barrier and be diverted downslope to the trench, and then be removed by a drain. Properties for the loam, clay and sand layers were obtained from Meyer (1993). Note that the permeability of the clay barrier is approximately thirty times larger than the U.S. Environmental Protection Agency (EPA) recommendation. However, in Hakonson et al. (1993) it was found to be quite difficult to install a clay barrier with this low permeability. In fact, a clay loam–bentonite mixture was used (Hakonson et al., 1993). The actual permeability of the installed cap was $\sim 30 \cdot 10^{-16}$ m^2 ($30 \cdot 10^{-7}$ cm s^{-1}).

The initial water table for this problem was at 10 m below the surface. This water table was maintained at the edge of the domain by specifying a constant pressure water boundary at the depth of 10 m. Infiltration was assumed to be 15 cm yr^{-1} uniformly along the top surface. Note from Fig. 2 that the drain is similar to the design used in Meyer (1993), where the sand layer is continued below the clay layer, and a drain is inserted as shown. The drain is modelled by seepage nodes.

In order to keep the waste dry, a pumping well is located at the center of the pyramid (see Fig. 1). This well is screened from a depth of 13.5 m to a depth of 16.5 m, with the pump being located at 16.5 m. This well is modelled using the Discrete Wellbore model. The well produces at 40 m^3 day^{-1}, with the constraint that the minimum pressure at the

Table 2
Fraction of total cumulative infiltration crossing the lower clay–sand barrier

Permeability of the clay barrier (m^2)	Fraction crossing the lower clay–sand interface
$30 \cdot 10^{-16}$	0.094
$9 \cdot 10^{-16}$	0.024
$3 \cdot 10^{-16}$	0.004

pump node cannot fall below 100 kPa (i.e. the pump is not permitted to become dry). The volume of the wellbore nodes was considered to be the actual wellbore volume (10-cm radius wellbore), with the wellbore permeability set at $1 \cdot 10^{-10}$ m^2. Increasing the wellbore permeability had no effect on the results.

Due to symmetry, only one quarter of the waste cover was simulated. A grid of 31 × 31 × 39 bricks was used, which were divided into tetrahedra as described in Letniowski and Forsyth (1991) (40,960 nodes). The spacing of the bricks in the x–y-direction was uniform at 1.333 m, while the spacing in the vertical direction was highly variable, with 1-cm spacing used near the upper clay–sand interface. This initial conditions for this problem were: water table at a depth of 10 m, and initial pressure of -1000 kPa above the water table. The simulation was run for 30 yr.

The interesting statistic is the fraction of the total cumulative infiltrating water which crosses the lower clay–sand interface after the entire 30-yr simulation period. Table 2 shows the fraction of infiltration crossing the barrier for various values of the clay permeability. It is clear that the performance of the barriers is very sensitive to the permeability of the clay barrier. As mentioned above, it may be difficult in practice to achieve the recommended permeability if $1 \cdot 10^{-16}$ m^2.

Fig. 3 shows the saturation contours in the sand layers immediately above and below the clay barrier, for the case with the clay permeability being $30 \cdot 10^{-16}$ m^2. Fig. 3 clearly shows the buildup of water saturation above the clay cap, and the much smaller saturation values in the sand layer below the clay cap.

This example demonstrates that a reasonably complicated problem with a variety of boundary conditions can be easily modelled using the approach described in this work.

8.2. *Five-spot two-phase problem*

This example is a well-known test case for which laboratory and numerical simulation results are known (Gaucher and Lindley, 1960; Coats et al., 1967; Wu et al., 1994). The computational domain consists of a one-quarter five spot, with constant-rate water injectors and constant liquid rate producers, as shown in Fig. 4.

A three-dimensional 11 × 11 × 6 brick grid is used for this problem, with $\Delta x = \Delta y = 14.22$ m and $\Delta z = 1.22$ m. The formation is treated as homogeneous and isotropic, and the wells are fully penetrating.

Detailed data for this example are given in Coats et al. (1967) and Wu et al. (1994). This problem was solved using the No Backflow model (Section 5.3), with both Full

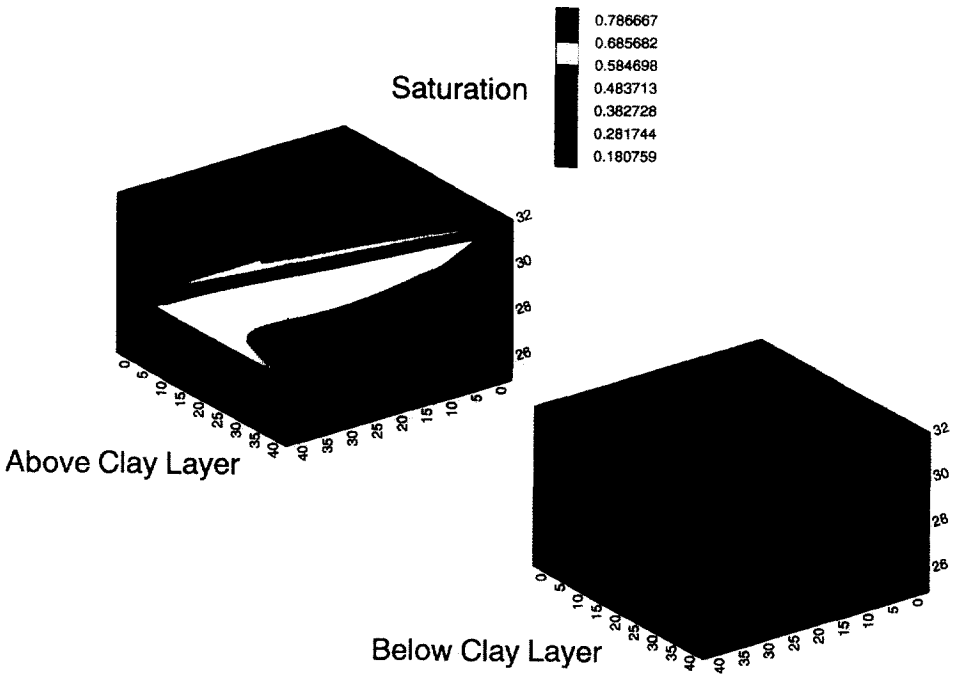

Fig. 3. Saturation contours at the layer immediately above the upper clay–sand interface, and the saturation contours at the layer immediately below the lower clay–sand interface.

Jacobian and Partial Jacobian (Section 7). For comparison, the Mobility Allocation model (see Eq. 25) was also used.

Fig. 5 shows the cumulative oil recovery curves for all three methods. The experimental results are also shown, as are the numerical results obtained by Coats et al. (1967). Note that all three methods give similar solutions. This is because the formation

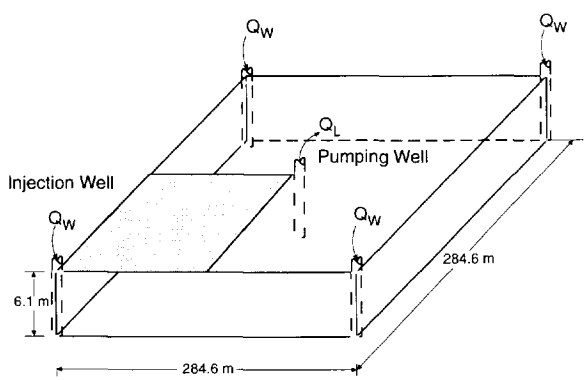

Fig. 4. Domain for two-phase five-spot problem.

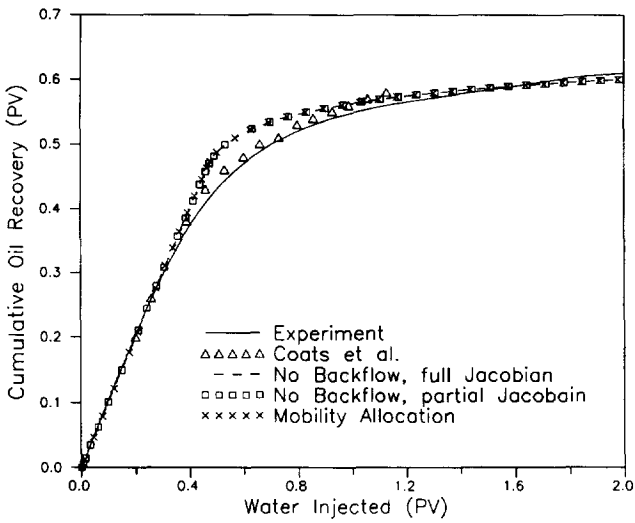

Fig. 5. Cumulative oil recovery for two-phase five-spot problem.

is homogeneous and isotropic, which is the best possible scenario for the Mobility Allocation method.

Table 3 give the total number of nonlinear iterations required for the entire simulation for each method. Since the overhead required for constructing and solving the Full Jacobian (as compared to the Partial Jacobian) is very small, the CPU time is roughly proportional to the nonlinear iteration count.

In this case, Table 3 clearly shows that the Partial Jacobian method is very poor in terms of numerical efficiency, requiring about three times the number of nonlinear iterations compared to the Full Jacobian technique. It is also interesting to see that the Mobility Allocation method required more nonlinear iterations than the more rigorous No Backflow Full Jacobian approach, even for this very simple problem.

8.3. Five-spot three-phase problem

Fig. 6 shows the domain for a layered three-dimensional problem, which consists of an air injector (constant rate at standard conditions) and constant-rate liquid producer. Both injectors and producers are screened over a 4-m length.

Table 3
Total nonlinear iterations for the two-phase five-spot problem

Method	Nonlinear iterations
No Backflow (Full Jacobian)	382
No Backflow (Partial Jacobian)	1,123
Mobility Allocation	447

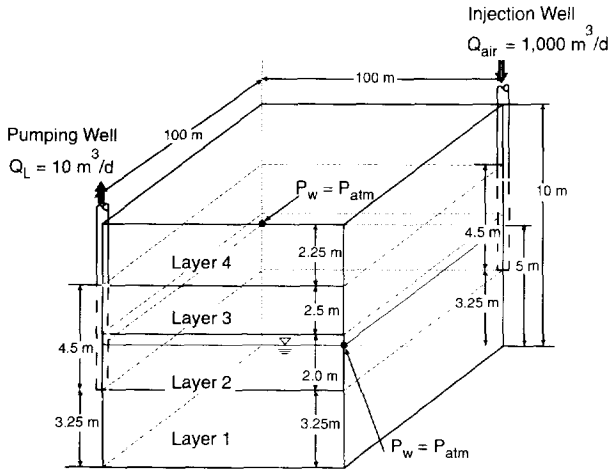

Fig. 6. Domain for air injection problem.

The computational domain is 100 m × 100 m × 10 m, and is discretized using a 11 × 11 × 21 grid. Node spacing in the x- and y-directions is a constant 10 m, while in the z-direction, the spacing is 0.5 m.

The air injector is located at $x = 100$ m, $y = 100$ m, $3.75 \le z \le 7.75$ m. Air is injected at 1000 m^3 day^{-1}. The producer is located at $x = y = 0.0$ m, $3.75 \le z \le 7.75$ m. The producer is constrained to produce a constant liquid rate of 10 m^3 day^{-1}.

The medium properties are expressed in terms of scaled van Genuchten (1980) relationships for three-phase flow:

$$\bar{S}_w = \frac{S_w - S_{wr}}{1 - S_{wr}} \tag{33a}$$

$$\bar{S}_a = \frac{S_a}{1 - S_{wr}} \tag{33b}$$

$$\bar{S}_n = \frac{S_n}{1 - S_{wr}} \tag{33c}$$

$$\bar{S}_L = \bar{S}_n + \bar{S}_w \tag{33d}$$

$$\bar{S}_{nr} = \frac{S_{nr}}{1 - S_{wr}} \tag{33e}$$

$$P_{cnw} = \frac{\sigma_{nw}\rho_w g}{\alpha\sigma_{aw}}\left[\left(\bar{S}_w\right)^{-1/\gamma} - 1\right]^{1/\beta} \tag{33f}$$

$$P_{can} = \frac{\sigma_{aw}\rho_w g}{\alpha\sigma_{aw}}\left[\left(1 - \bar{S}_a\right)^{-1/\gamma} - 1\right]^{1/\beta} \tag{33g}$$

Table 4
Material properties for three-phase five-spot problem

Layer	$K_x = K_y = K_z$ (m^2)	ϕ	S_{wr}	α (m^{-1})	β
1	$2.15 \cdot 10^{-11}$	0.314	0.0396	6.62	1.39
2	$3.95 \cdot 10^{-13}$	0.333	0.0869	3.99	1.56
3	$1.43 \cdot 10^{-12}$	0.379	0.1098	3.54	3.06
4	$2.44 \cdot 10^{-11}$	0.279	0.1026	7.24	1.60

Table 5
Fluid properties for three-phase five-spot problem

Fluid	Density ($kg\ m^{-3}$)	Viscosity (Pa s)	Compressibility (Pa^{-1})
Water	1,000	1.0	$1 \cdot 10^{-10}$
NAPL	800	0.969	$1 \cdot 10^{-10}$
Air	1.177	$1.98 \cdot 10^{-2}$	Ideal Gas law

$$P_{caw} = \frac{\rho_w g}{\alpha}\left[\left(1 - \bar{S}_a\right)^{-1/\gamma} - 1\right]^{1/\beta} \tag{33h}$$

$$k_{rw} = \left(\bar{S}_w\right)^{1/2}\left[1 - \left\{1 - \left(\bar{S}_w\right)^{1/\gamma}\right\}^{\gamma}\right]^2 \tag{33i}$$

$$k_{rn} = \left(\bar{S}_n - \bar{S}_{nr}\right)^{1/2}\left[\left\{1 - \left(\bar{S}_w\right)^{1/\gamma}\right\}^{\gamma} - \left\{1 - \left(\bar{S}_L\right)^{1/\gamma}\right\}^{\gamma}\right]^2 \tag{33j}$$

$$k_{ra} = \left(\bar{S}_a\right)^{1/2}\left[1 - \left(\bar{S}_L\right)^{1/\gamma}\right]^{2\gamma} \tag{33k}$$

where S_{wr} is the residual water saturation; S_{nr} is the residual nonaqueous (NAPL) saturation; σ_{nw}, σ_{an} and σ_{aw} are the interfacial tensions between the NAPL, water and air phases, respectively; and P_{cnw} and P_{can} are the NAPL–water and air–NAPL capillary pressures, respectively. This problem has four layers, with layer properties given in Table 4. Fluid properties are given in Table 5. Initial conditions for this problem are generated by placing a layer of NAPL 2.5 m in height along the water table.

After the system was equilibrated, air injection and liquid production were carried out for one year. Other boundary conditions are illustrated in Fig. 6.

This problem was solved using the No Backflow model as described in Section 5.3. Both a fully coupled, full Newton method and a Partial Jacobian method (see Section 7) were used. We also used the Mobility Allocation method (Section 5.4). Fig. 7 shows the cumulative NAPL recovery for all three methods. Both Full and Partial Jacobian methods give essentially the same solution. This is, of course, not surprising since both methods are solving the same discrete equations, but using a different method to solve these equations. However, in this case, the Mobility Allocation method produces quite different results. This is not unexpected, since the assumptions made in the Mobility Allocation method will be significantly in error for layered systems.

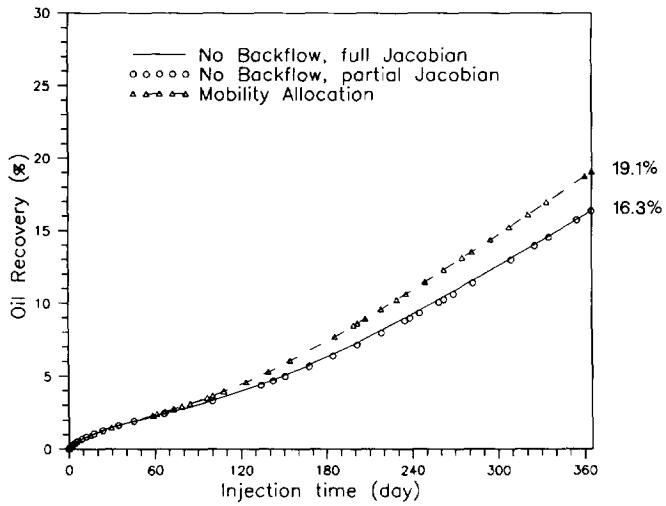

Fig. 7. Cumulative NAPL recovery (%) for the three methods, five-spot air injector.

The work required for each method is roughly proportional to the number of nonlinear iterations, since the overhead required for solving the full (as opposed to partial) Jacobian is very small. Table 6 gives the total number of nonlinear iterations for each method for the entire one year of air injection.

Table 6 indicates that the *Partial Jacobian* method results in significant degradation in performance. We can also see that the Mobility Allocation method, as well as giving erroneous solutions, requires about 60% more nonlinear iterations than the No Backflow, Full Jacobian Method.

8.4. Multiphase seepage face

Fig. 8 shows the computational domain for a two-dimensional cross section. Note the seepage face boundary on the right-hand edge. This condition is modeled using the method described in Section 6. Three grids (coarse, medium, fine) were used to simulate this case. The finest grid is shown in Fig. 9. Relative permeability and capillary pressure data are given in Tables 7 and 8.

Stone's second method is used for the three-phase NAPL relative permeability (Tables 7 and 8). The porosity ϕ was set at $\phi = 0.28$, while the absolute permeability was $K_x = K_y = 1.019 \cdot 10^{-11}$ m^2. Other fluid data are given in Table 9.

Table 6
Total nonlinear iterations for the five-spot air injection problem

Method	Nonlinear iterations
No Backflow (Full Jacobian)	511
No Backflow (Partial Jacobian)	677
Mobility Allocation	830

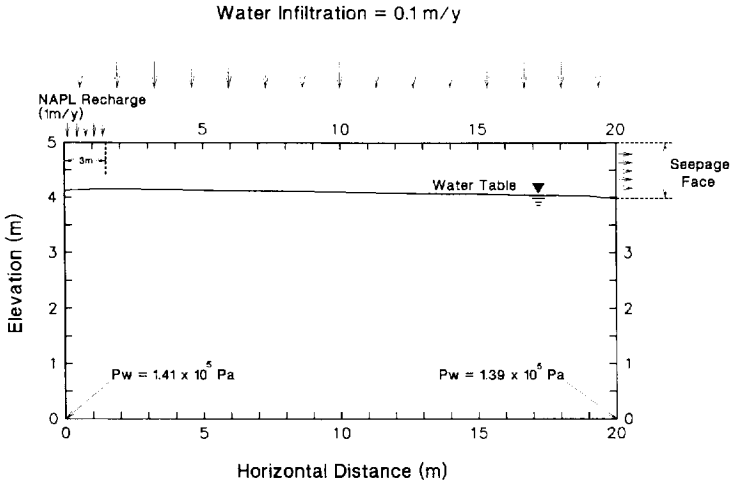

Fig. 8. Domain for the seepage face problem.

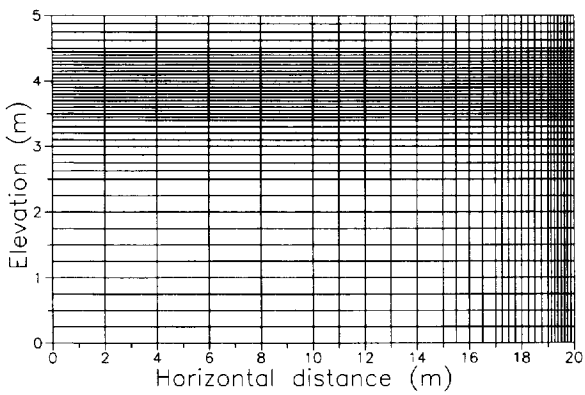

Fig. 9. Fine grid for the seepage face problem.

Table 7
NAPL–water data for the seepage face problem

S_w	k_{rw}	k_{rn}	P_{cnw} (kPa)
0.2	0.0	0.68	9.0
0.3	0.04	0.55	5.4
0.4	0.1	0.43	3.9
0.5	0.18	0.31	3.3
0.6	0.3	0.2	3.0
0.7	0.44	0.12	2.7
0.8	0.6	0.05	2.4
0.9	0.8	0.0	1.5
1.0	1.0	0.0	0.0

Table 8
NAPL–air data for the seepage face problem

S_a	k_{ra}	k_{rn}	P_{can} (kPa)	P_{caw} (kPa)
0.0	0.0	0.68	0.0	0.0
0.1	0.01	0.49	0.9	1.0
0.2	0.04	0.34	1.2	2.0
0.3	0.09	0.21	1.5	3.0
0.4	0.16	0.116	1.8	3.3
0.5	0.25	0.045	2.1	3.6
0.6	0.36	0.0009	2.4	3.9
0.68	0.46	0.0	3.0	4.5
0.8	0.64	0.0	9.0	6.6

Table 9
Fluid data for the seepage face problem

Fluid	Density (kg/m^{-3}) (at standard conditions)	Viscosity (Pa s)
Water	1,000	1.139
NAPL	800	2.0
Air	1.177	0.0198

Initially, the NAPL saturation was zero everywhere in the domain, and the model (with no NAPL injection) was run to steady state. Then, NAPL was injected for one year (1 m yr^{-1}) as shown in Fig. 8. NAPL injection then ceased, and the problem was again run to steady state ($\sim$ 10 yr).

Fig. 10, Fig. 11, Fig. 12 show the NAPL saturation contours at one year for the coarse, medium and fine grids, respectively. Note the large region where $S_n \approx 0.1$ (the

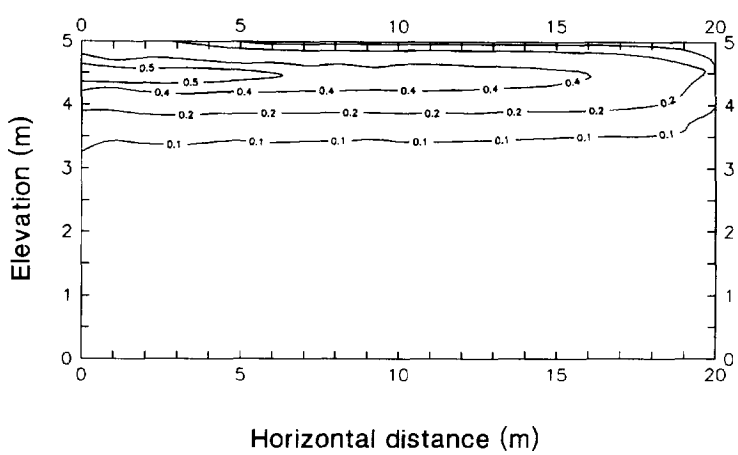

Fig. 10. Coarse grid saturation contours, seepage face problem.

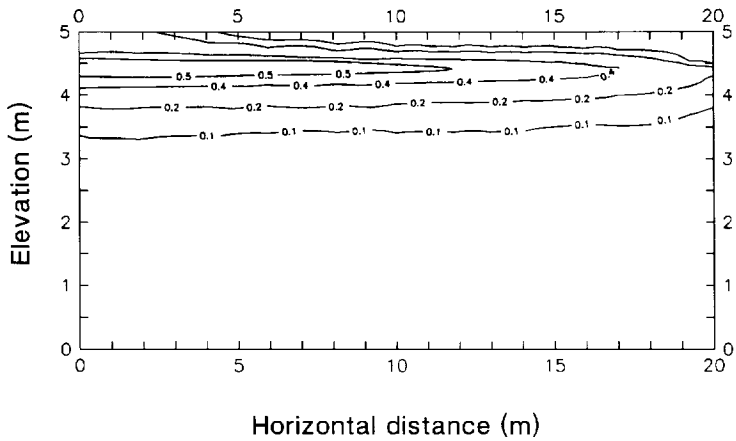

Fig. 11. Medium grid saturation contours, seepage face problem.

residual value) near the seepage face. This is due to the outlet effect, which will be discussed below.

The total water seepage flux and total NAPL seepage flux are shown in Figs. 13 and 14. Note that the water flux decreases sharply as the NAPL flux increases.

In Section 6, we argued that the source/sink terms for seepage face nodes of the form given by Eqs. 30 will not permit liquid to flow out, until the liquid saturation is ~ 1.0. This is in fact observed in the computation.

Close examination of the source/sink terms reveals that (on the finest grid) water only flows out from the lowest seepage face node. However, water and NAPL flow out from the four higher seepage face nodes. At first sight, it is difficult to understand why two simultaneous flow of water and NAPL at the seepage face is observed.

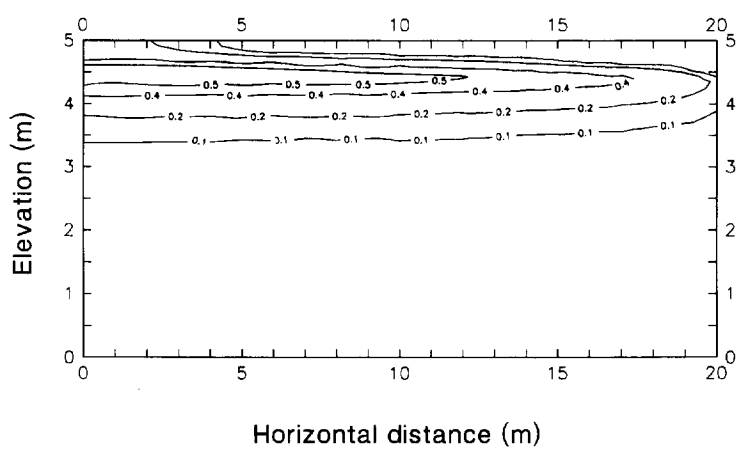

Fig. 12. Fine grid saturation contours, seepage face problem.

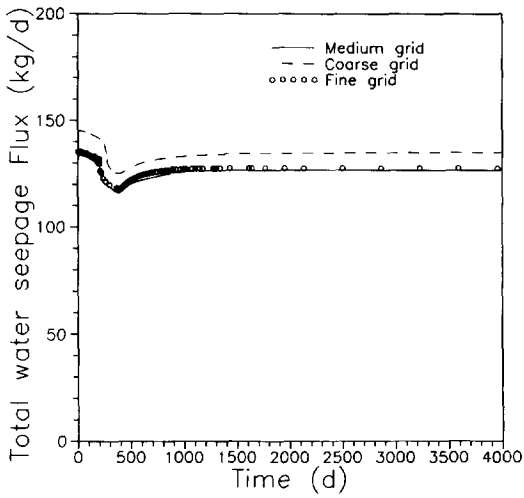

Fig. 13. Water seepage face flux.

Consider a seepage face node i which is liquid saturated, and both NAPL (S_{ni}) and water (S_{wi}) saturations are well above their respective residual values (i.e. relative permeabilities for water and NAPL $\gg 0$). In this case, due to the form of Eqs. 30,

$$P_{ni} \approx P_{ab} \tag{34a}$$

$$P_{wi} \approx P_{ab} - P_{cnw}(S_w = S_{wi}) \tag{34b}$$

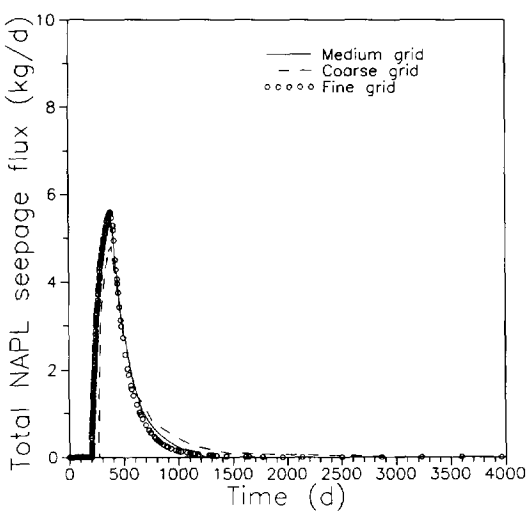

Fig. 14. NAPL seepage face flux.

Assuming that the water–NAPL capillary pressure is non zero at $S_w = S_{wi}$, then:

$$(P_{ab} - P_{wi}) > 0 \tag{35}$$

which, from Eq. 30a implies that water cannot flow out. In this case, only NAPL can exit the system through the seepage node.

However, if the NAPL saturation is reduced to near the residual value, i.e. $S_{ni} = S_{nri} + \epsilon$, then the relative permeability of the NAPL phase will be very small, and it can no longer be assumed that $P_{ni} \approx P_{ab}$. However, since the water relative permeability will not be small at this water saturation, then:

$$P_{wi} \approx P_{ab} \tag{36a}$$

$$P_{ni} \approx P_{ab} + P_{cnw}(S_w = 1.0 - S_{nri}) \tag{36b}$$

The amount of fluid leaving the seepage node should converge as the parameter LARGE $\to \infty$ in Eqs. 27 and 30. Now,

$$(P_{ab} - P_{wi}) \to 0 \quad \text{as} \quad WP_i' \to \infty \tag{37}$$

so that

$$WP_i' \lambda_{wi} \rho_{wi} (P_{ab} - P_{wi}) \tag{38}$$

approaches a finite limit. Similarly,

$$\left.\begin{aligned} S_{ni} &\to S_{nr} \\ \lambda_n &\to 0 \\ (P_{ab} - P_{ni}) &\to P_{cnw}(S_w = 1.0 - S_{nri}) \end{aligned}\right\} \quad \text{as} \quad WP_i' \to \infty \tag{39}$$

so that

$$WP_i' \lambda_{ni} \rho_{ni} (P_{ab} - P_{ni}) \tag{40}$$

approaches a finite quantity.

Consequently, simultaneous flow of NAPL and water at a seepage node can occur only if the capillary pressure is reduced to (nearly) the minimum possible value. This was pointed out in Settari (1973), and this is what is observed in our simulations: both phases flow only when the NAPL saturation is almost at the residual value.

We emphasize once again that this effect only occurs because the NAPL saturation is near residual. Consequently, the NAPL pressure is no longer equal to atmospheric pressure, at a point infinitesimally inside the porous medium. More precisely, there is a thin layer near the outlet where the NAPL saturation rapidly decreases to almost the residual value. Although the pressure gradient is large in this layer, the mobility of the NAPL is small.

In fact, it could be argued that the same effect will occur for liquid air flow, i.e. as the air saturation decreases to near zero, there could be simultaneous flow of air and liquid, since the air pressure cannot be assumed to be equal to atmospheric pressure. However, this would mean that the air pressure inside the domain would be significantly higher than the atmospheric pressure. Since the viscosity of the air phase is very small, this would result in enormous gas-phase velocities. In all our tests with realistic

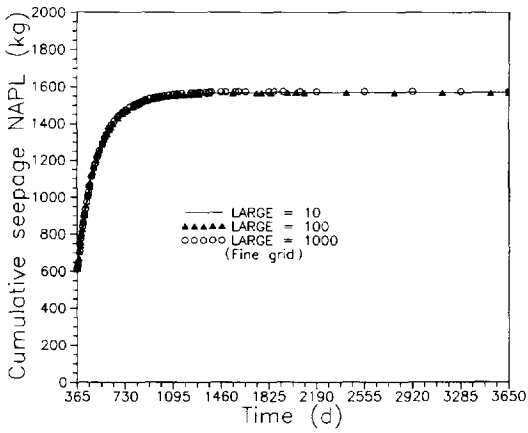

Fig. 15. Cumulative NAPL through the seepage face for different values of LARGE.

remediation scenarios, we have never seen numerically significant simultaneous flow of air and liquid from a seepage face node.

In order to verify that the solution is independent of LARGE (in Eq. 27), we carried out several fine grid runs with different values of this parameter. Fig. 15 shows the total cumulative NAPL produced from the seepage face from 1 to 10 yr, for various values of LARGE. Clearly, when LARGE is sufficiently large, the cumulative NAPL converges to a value independent of LARGE.

Another way of understanding the source/sink technique for multiphase seepage boundary conditions is to imagine formulating the boundary conditions by using a very fine mesh near the seepage face. For simplicity of exposition, we will assume that the air-phase saturation is zero ($S_a = 0$), and that a two-dimensional Cartesian grid system is being used, with the seepage face along the z-axis. In this case, we set the water and NAPL pressures (at the boundary) to the boundary air pressure P_{ab}. Let node i be the node adjacent to a boundary seepage face node (in the x-direction). The NAPL and water fluxes through the seepage node are given by:

$$q_{li} = \frac{A}{\Delta x} \lambda_{li} \rho_{li} \min[0,(P_{ab} - P_{li})] \quad (l = \mathrm{w}, \mathrm{n}) \tag{41}$$

where

A = (discrete flow area)

Δx = (mesh size in the x − direction)

which is simply the flux computed by using the discrete normal derivative of the pressures. Now, imagine taking the limit as $\Delta x \to 0$. If there is mobile water at the seepage face (which is the case in our example), then the only way that Eq. 41 can yield a finite limit for q_{wi} is for:

$$P_{wi} \to P_{ab} \quad \text{as} \quad \Delta x \to 0 \tag{42}$$

Since the NAPL pressure tends to:

$$P_{ni} \rightarrow P_{ab} + P_{cnw}(S_{wi}) \tag{43}$$

where $P_{cnw}(S_{wi})$ is generally non zero, this means that the only way Eq. 41 can give a finite limit for q_{ni}, is for:

$$\left.\begin{array}{l} S_{ni} \rightarrow S_{nr} \\ \lambda_{ni} \rightarrow 0 \end{array}\right\} \quad \text{as} \quad \Delta x \rightarrow 0 \tag{44}$$

Note that the NAPL pressure gradient actually tends to infinity at the seepage boundary, but that the flux tends to a finite value.

Observe also that if in Eqs. 30 we replace:

$$\mathrm{WP}_i' \leftarrow \frac{A}{\Delta x} \tag{45}$$

then Eqs. 30 and 41 become formally identical. In other words, the use of:

$$\mathrm{WP}_i' = \mathrm{WP}_i * \mathit{LARGE} \quad (\mathrm{LARGE} \rightarrow \infty) \tag{46}$$

simulates the effect of using a very fine mesh near the boundary. Note that Figs. 13 and 14 indicate that the seepage fluxes for the medium mesh have essentially converged to the final values.

9. Conclusions

We have presented a conceptually simple and easy to implement method for handling various boundary conditions in multiphase subsurface flow.

Multinode, constant-rate wells can be handled with varying levels of sophistication. The most accurate method uses a discretized wellbore to simulate flow in the wellbore. This method predicts liquid levels in the wellbore, and can be used in backflowing situations. If precise liquid levels in the well are not important, but backflow may occur, then the wellbore can be replaced by a single virtual node. Finally, if backflow can be assumed not to occur (which is probably the most common case), then a single total flow constraint equation is added to the discrete nonlinear equations, and a unknown wellbore pressure is added to the set of unknowns (for each distinct well).

Computational examples show that ignoring some of the terms in the Jacobian for multinode wells can drastically increase the number of nonlinear iterations required for convergence. In some cases, about three times as many nonlinear iterations are required if a Partial Jacobian is used compared to a Full Jacobian where all terms are taken into account. Since CPU time is roughly proportional to nonlinear iteration count, dropping terms in the Jacobian is ill-advised.

A simple method borrowed from the petroleum literature based on Mobility Allocation for multinode wells has been shown to produce large errors in some situations. In cases where the Mobility Allocation approximation produces small errors, the number of nonlinear iterations is larger than a full Newton solution of the more rigorous wellbore model. Consequently, there does not seem to much point in using the Mobility Allocation method.

In all cases, we have taken the capillary pressure into account at source/sink locations. This contrasts with the models typically used in the petroleum industry, where capillary pressure effects at source/sink locations are ignored. While this is a reasonable approach for petroleum industry applications, this is generally not applicable for near-surface flows. In particular, we have demonstrated how the source/sink method can be used to simulate the complex behaviour which occurs for multiphase flow near a seepage face. In this case, it is absolutely essential to take into account capillary pressure outlet effects. The method developed in this work can be shown to be equivalent to the result obtained by using an infinitesimally small mesh near the seepage boundary. For interesting cases where simultaneous flow of NAPL and water occurs, there is a very thin layer near the seepage face where the NAPL saturation decreases sharply to near the residual value. A mesh refinement study showed that the source/sink method can predict the NAPL and water-phase fluxes even at fairly coarse grid sizes.

In all cases, a mathematically correct approach is used with the source/sink method: fluid properties can be specified for ingoing components, fluid properties are not specified for outgoing components.

Acknowledgements

This work was supported by the National Sciences and Engineering Research Council of Canada, by the Information Technology Research Center, funded by the Province of Ontario, and by HydroGeoLogic, Inc.

References

Abriola, L. and Pinder, G., 1985. A multiphase approach to the modelling of porous media contamination by organic compounds, 1. Equation development. Water Resour. Res., 29: 1697–1708.

Aziz, K. and Settari, A., 1979. Petroleum Reservoir Simulation. Academic Press, New York, NY.

Coats, K., Nielson, R., Terhune, M. and Weber, A., 1967. Simulation of three dimensional, two-phase flow in oil and gas reservoirs. Soc. Pet. Eng. J., 7: 377–388.

Collins, D., Nghiem, L., Sharma, R. and Li, Y., 1992. Field scale simulation of horizontal wells. J. Can. Pet. Technol., 31: 14–21.

D'Azevedo, E., Forsyth, P. and Tang, W., 1992. Towards a cost effective ILU preconditioner with high level fill. BIT, 32: 442–463.

Falta, R., Javandel, I., Pruess, K. and Witherspoon, P., 1989. Density driven flow of gas in the unsaturated zone due to evaporation of volatile organic compounds. Water Resour. Res., 25: 2159–2169.

Falta, R., Pruess, K., Javandel, I. and Witherspoon, P., 1992. Numerical modelling of steam injection for the removal of nonaqueous phase liquids from the subsurface, 1. Numerical formulation. Water Resour. Res., 28: 433–449.

Faust, C., Guswa, J. and Mercer, J., 1989. Simulation of three dimensional flow of immiscible fluids within and below the unsaturated zone. Water Resour. Res., 25: 2449–2464.

Forsyth, P., 1988. Simulation of nonaqueous phase groundwater contamination. Adv. Water Res., 11: 74–83.

Forsyth, P., 1991. A control volume finite element approach to NAPL groundwater contamination. SIAM (Soc. Ind. Appl. Math.) J. Sci. Stat. Comput., 12: 1029–1057.

Forsyth, P., 1993. A positivity preserving method for simulation of steam injection for NAPL site remediation. Adv. Water. Res., 16: 351–370.

Forsyth, P., 1994. Three dimensional modelling of steam flush for DNAPL site remediation. Int. J. Numer. Meth. Fluids, pp. 1055–1081.

Forsyth, P. and Shao, B., 1991. Numerical simulation of gas venting for NAPL site remediation. Adv. Water Res., 14: 354–367.

Forsyth, P., Wu, Y. and Pruess, K., 1995. Robust numerical methods for saturated–unsaturated flow with dry initial conditions in heterogeneous media. Adv. Water. Res., 18: 25–37.

Fung, L., Hiebert, A. and Nghiem, L., 1992. Reservoir simulation with a control volume finite element method. Soc. Pet. Eng. J. Res. Eng., pp. 349–357.

Gaucher, D. and Lindley, C., 1960. Waterflood performance in a stratified five spot reservoir, a scaled model study. Trans. AIME (Am. Inst. Min. Metall. Eng.) Pet. Eng, 219: 208–215.

Hakonson, T., Bostick, K., Trujillo, G., Manies, K., Warren, R., Lane, L., Kent, J. and Wilson, W., 1993. Hydrologic evaluation of four landfill cover designs at Hill Air Force Base, Utah. Los Alamos Natl. Lab., Los Alamos, NM, Rep. LA-UR-93-4469.

Huyakorn, P., Thompson, S. and Thompson, B., 1984. Techniques for making finite element methods competitive in modelling flow in variably saturated porous media. Water Resour. Res., 20: 1099–1115.

Kaluarachchi, J. and Parker, J., 1989. An efficient finite element method for modelling multiphase flow. Water Resour. Res., 25: 43–54.

Letniowski, F. and Forsyth, P., 1991. A control volume finite element method for three dimensional NAPL groundwater contamination. Int. J. Numer. Meth. Fluids, 13: 955–970.

Meyer, P., 1993. Application of an infiltration evaluation methodology to a hypothetical low-level waste disposal facility. U.S. Nucl. Regulat. Comm., Washington, DC, Rep. NUREG/CR-6114, PNL-8842.

Panday, S., Forsyth, P., Falta, R., Wu, Y. and Huyakorn, P., 1995. Considerations for robust compositional simulation of subsurface NAPL contamination and remediation. Water Resour. Res., 31: 1273–1289.

Peaceman, D., 1983. Numerical interpretation of well-block pressures in numerical reservoir simulation with nonsquare grid blocks and anisotropic permeability. Soc. Pet. Eng. J., pp. 531–543.

Peaceman, D., 1990. Interpretation of wellblock pressures in numerical reservoir simulation, Part III. Off center and multiple wells within a wellblock. Soc. Pet. Eng. J. Res. Eng., pp. 227–232.

Sammon, P., 1988. An analysis of upstream weighting. Soc. Pet. Eng. J. Res. Eng., 3: 1053–1056.

Settari, A., 1973. Numerical simulation of three phase coning in petroleum reservoirs. Ph.D. Thesis, Department of Mechanical Engineering, University of Calgary, Calgary, Alta.

Sleep, B. and Sykes, J., 1993. Compositional simulation of groundwater contamination by organic compounds 1. Model development and verification. Water Resour. Res., 29: 1697–1708.

Unger, A., Forsyth, P. and Sudicky, E., 1996. Variable spatial and temporal weighting schemes for use in multiphase compositional problems. Adv. Water Res., 19: 1–28.

van der Vorst, H., 1992. Bi-CGSTAB: A fast and smoothly converging variant of Bi-CG for the solution of nonsymmetric linear systems. SIAM (Soc. Ind. Appl. Math.) J. Sci. Stat. Comp., 13: 631–645.

van Genuchten, M.Th., 1980. A closed form equation for predicting the hydraulic conductivity of unsaturated soils. Soil. Sc. Soc. Am. J., 44: 892–898.

Wu, Y., Huyakorn, P. and Park, N., 1994. A vertical equilibrium model for assessing nonaqueous phase liquid contamination and remediation of groundwater systems. Water Resour. Res., 30: 903–912.